REVIEW

VIEW

Oxygen-derived free radicals: Production, biological importance, bioimaging, and analytical detection with responsive luminescent nanoprobes

Jianping Liu | **Miaomiao Wu** | **Run Zhang** | **Zhi Ping Xu**

Australian Institute for Bioengineering and Nanotechnology, The University of Queensland, St Lucia, Queensland, Australia

Correspondence
Run Zhang and Zhi Ping Xu, Australian Institute for Bioengineering and Nanotechnology, The University of Queensland, St. Lucia, Queensland 4072, Australia.
Email: r.zhang@uq.edu.au; gordonxu@uq.edu.au

Jianping Liu and Miaomiao Wu contributed equally to this work.

Abstract

Oxygen-derived free radicals (ODFRs) are partially reduced oxygen reactive intermediates in living organisms during various biological processes, such as mitochondrial respirations, enzyme-catalyzed oxidations, and radiolysis. Of various ODFRs being identified, superoxide anion ($O_2^{•-}$) and hydroxyl (•OH) radicals are extensively investigated. Due to their high reactivity, these radicals can oxidize many biomolecules, including nucleic acids, proteins, lipids, and carbohydrates, which would damage some key cellular components. Under oxidative stress, elevated oxygen radical levels are closely associated with various diseases, such as neurodegenerative diseases, cardiovascular diseases, rheumatoid arthritis, and cancers. In this context, a number of responsive nanoprobes have been developed for luminescent detection of ODFRs in living organisms. In this review, we briefly introduce the production of ODFRs and their biological importance for various diseases. We then extensively summarize responsive nanoprobes for detection and bioimaging of these two oxygen radicals, $O_2^{•-}$ and •OH, which are designed and developed based on their specific oxidation mechanisms in the recent decade. Challenges and some future research directions are also proposed as the conclusion.

KEYWORDS
luminescence biosensing and imaging, oxygen-derived free radical, radical-associated diseases, responsive nanoprobes, superoxide anion and hydroxyl radical

1 | INTRODUCTION

As the electron paramagnetic resonance study by Commoner et al. in 1954 presented the first evidence of free radicals in the biology system,[1] there is growing interest in the role of reactive oxygen species (ROS) in cells and tissues, due to the pivotal implication in various physiological and pathological conditions. ROS are a group of highly reactive oxidation-state species that are produced by incomplete reduction of oxygen molecules. Examples of ROS include superoxide anion ($O_2^{•-}$), hydroxyl radical (•OH), singlet oxygen ($^1O_2$), hydrogen peroxide (H_2O_2), and hypochlorite (OCl^-).[2] ROS act as a double-edged sword in various cellular processes. At low

concentrations, ROS are critical for receptor-mediated signal pathways and transcription activations.[3,4] However, abnormal elevated ROS levels in cells may lead to cellular dysfunction, induce pathological changes, and contribute to the development of diseases, such as cancerous, inflammasome, and neurodegenerative diseases.[5,6] This paradox suggests that the amount of reactive species determines their roles in vivo, shifting from beneficial to detrimental.

Of various ROS, oxygen-derived free radicals (ODFRs), mainly including $O_2^{\bullet-}$ and $\bullet OH$ radicals, are regarded as the most crucial members with a serious threat to the chemical integrity of cells due to their high concentration and activity in comparison with other ROS. Consequently, remarkable progress has been made to develop reaction-based nanoprobes for luminescent monitoring of $O_2^{\bullet-}$ and $\bullet OH$ in terms of high sensitivity, excellent selectivity, and minimal invasiveness.[7–9] These responsive nanoprobes are able to visualize the local $O_2^{\bullet-}$ and $\bullet OH$ and track their concentration changes in living cells and organisms.

In this review, the formation, molecular targets, and biological activities of free radicals are first elaborated for a better understanding of ROS participation in various disease conditions. Furthermore, considering the demand for luminescent detection and imaging of these radical species in living cells and organisms, we summarize the recent advances of responsive nanoprobes that can indicate the production sites and level changes of $O_2^{\bullet-}$ and $\bullet OH$. This review aims to provide a general overview of ODFRs detection and imaging methods, and offer more insights for the future design of oxidative species selective and oxidative-sensitive nanoprobes.

2 | ORIGIN AND BIOLOGICAL EFFECTS OF OXYGEN-DERIVED FREE RADICALS

ROS are a group of highly reactive chemical species produced during the biological metabolic processes.[10] The free radicals that can be produced in biological systems include superoxide ($O_2^{\bullet-}$), hydroxyl ($\bullet OH$), oxygen radical ($O_2^{\bullet\bullet}$), alkoxyradical ($\bullet OR$), and peroxyl radical ($\bullet OOR$). Of these ODFRs, $O_2^{\bullet-}$ and $\bullet OH$ radicals are most extensively studied. These two ODFRs are essential biospecies in living cells and organisms, but their imbalanced levels in living organisms are implicated in various diseases, such as neurodegenerative diseases, cardiovascular diseases (CVD), rheumatoid arthritis (RA), and cancers.[11] Under oxidative stress conditions, elevated intracellular levels of ODFRs cause oxidation of lipids, proteins, and nucleic acids (Scheme 1).[12] In this section, the production of $O_2^{\bullet-}$ and $\bullet OH$ radicals, their oxidation with biomolecules, and the relationship with various diseases are briefly summarized.
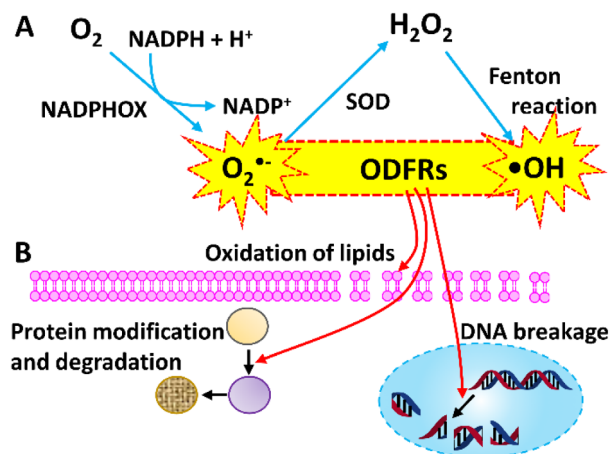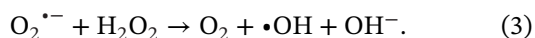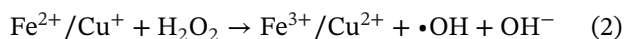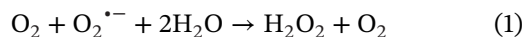

SCHEME 1 Schematic illustration of the production of ODFRs ($O_2^{\bullet-}$ and $\bullet OH$ in this review) (A) and their reactions with biomolecules, including lipids, proteins, and nucleic acids (B)

2.1 | Sources of oxygen-derived free radicals

ODFRs can be generated from exogenous or endogenous sources. The external sources of free radicals are various, such as air/water pollution, cigarette smoking, ultraviolet light, alcohol, and ionizing radiation.[13,14] The endogenous sources mainly refer to enzymatic cell metabolism in mitochondria, peroxisomes, and endoplasmic reticulum, where oxygen consumption mostly occurs. In fact, most oxygen molecules are handled by the cytochrome oxidase, an enzyme in the mitochondria, which is able to transfer four electrons to O_2 to form two stable H_2O molecules.[15] However, the transfer of less than four electrons in the reduction of oxygen molecule is prone to the generation of active oxygen products. For example, $O_2^{\bullet-}$ is produced via an enzyme-catalyzed reaction (including cytoplasmic membrane NADPH oxidase, enzyme complex of the mitochondrial respiratory chain, xanthine oxidase, peroxidases, and cytochromes P450) and by a nonenzymatic process, in which only one electron is transferred to molecular oxygen. $O_2^{\bullet-}$, as the most critical and widespread free radical in living organisms, participates in the formation of other ROS, such as hydrogen peroxide (H_2O_2) and hydroxyl radical ($\bullet OH$).

H_2O_2 is produced in living organisms through a dismutation reaction with the catalysis of the enzyme superoxide dismutase (SOD) (Equation 1). H_2O_2 is not a free radical and is supposed to be less reactive than radical species. However, H_2O_2 is able to react with transition metals, such as Fe^{2+} and Cu^+, to produce highly reactive radical species (e.g., $\bullet OH$) or activated metal complexes.[16] $\bullet OH$ is one of the most reactive free radicals that can quickly react with biomolecules such as DNA bases, amino acids, sugars,

and phospholipids after its generation. •OH is produced via two reactions, that is, Fenton reaction (Equation 2), a reaction between H_2O_2 and Fe^{2+}/Cu^+, and Haber–Weiss reaction (Equation 3), where an excess of $O_2^{•-}$ reacts with H_2O_2. •OH radical attacks biological substrates via electron abstraction, hydrogen abstraction, and double-bond addition, resulting in more fatal damages to normal cells than any other ROS[17–20]:

$$O_2 + O_2^{•-} + 2H_2O \rightarrow H_2O_2 + O_2 \qquad (1)$$

$$Fe^{2+}/Cu^+ + H_2O_2 \rightarrow Fe^{3+}/Cu^{2+} + •OH + OH^- \quad (2)$$

$$O_2^{•-} + H_2O_2 \rightarrow O_2 + •OH + OH^-. \qquad (3)$$

2.2 | Oxidative damage to cellular components

Generally, a moderate level of oxygen free radicals is necessary to human health.[21] Even if the levels of these free radicals increase in some circumstances, antioxidants in the defense system can prevent, reduce, and repair the free radical-induced damages. The physiological defenses include enzymatic scavengers (SOD, peroxidase, and catalase), nonenzymatic scavengers (tocopherol, ascorbic acid, and biothiols),[22] and protections of some exogenous compounds, all of which inactivate oxygen radicals and their secondary free radicals.[23] For example, SOD converts $O_2^{•-}$ to H_2O_2 and O_2 (Equation 4) and peroxidase/catalase converts H_2O_2 to water and O_2 (Equation 5). However, when antioxidant activities in biological system cannot counteract the excess of free radicals, these reactive oxidants lead to a phenomenon named oxidative stress.[24] Overwhelming free radicals can severely oxidize the cell membrane and cellular components, including lipids, proteins, nucleic acids, and carbohydrates:

$$2H^+ + O_2^{•-} \rightarrow H_2O_2 + O_2 \qquad (4)$$

$$2H_2O_2 \rightarrow O_2 + 2H_2O. \qquad (5)$$
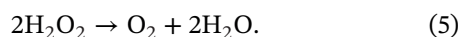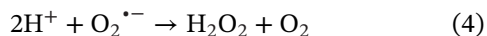
2.2.1 | Effect on nucleic acids

As one of the highly ROS (hROS, including •OH, hypochlorous acid (HOCl), and peroxynitrite ($ONOO^-$)), •OH directly attacks purine and pyrimidine as well as deoxyribose sugar backbone in DNA and leads to different oxidative DNA lesions such as base and sugar modification, strand breaks, base-free sites, and DNA–protein crosslinking.[25] Of the oxidation products, 8-hydroxy-deoxyguanosine (8-OHdG) has been found to be a criti-

cal biomarker of DNA damage and involved in the development and progression of CVD.[26,27] In comparison with DNA, single-stranded RNA in cytoplasm is subjected to more severe oxidative damage in the body.[28] Among RNA damage products, 7,8-dihydro-8-oxoguanosine (8-oxoG) is most extensively studied and its excessive amount induces a variety of pathologies such as Parkinson's disease (PD),[29] Alzheimer's disease (AD),[30] and atherosclerosis.[31]

2.2.2 | Effect on lipids

The membrane lipids, especially the polyunsaturated fatty acid residues of phospholipids, undergo peroxidation as consequence of the free radical action.[32] Once lipid peroxidation is initiated, the lipid radical reacts with molecular oxygen to produce a lipid peroxyl radical and spreads rapidly to the other lipid molecules as a chain reaction. A series of oxidative reactions trigger membrane breakdown and cell death. Malondialdehyde and 4-hydroxylnonenal (4-HNE) as final products of lipid peroxidation are of toxicological interest to the DNA and proteins.[33–36]

2.2.3 | Effect on proteins

Oxygen radicals can attack different amino acids in proteins, leading to the production of different oxidation products. For example, after the oxidation, lysine changes to a-aminoadipic semialdehyde, tryptophan to kynurenine, and leucine and valine residues to hydroxyl residues.[37] The ROS oxidation leads to the changes of protein structures and the inactivation of enzyme activity, thus suppressing the normal metabolism process.[38] Protein carbonyl is considered as the biomarkers of protein oxidation and its level is raised in neurological diseases,[39,40] RA,[41] and other pathological conditions.[42]

2.2.4 | Effect on carbohydrates

Oxygen radicals such as •OH can lead to the formation of a carbon-centered radical via randomly abstracting an H atom from any C-H bonds. This activity brings about fragmentation of carbohydrates, such as hyaluronic acid.[43] Hyaluronic acid is a glycosaminoglycan and can be depolymerized by neutrophils-stimulated free radicals in RA.[44]

2.3 | Oxidative stress and diseases

Oxidative damage to the critical biomolecules is implicated in many pathological conditions such as

neurodegenerative disease,[45] acute pancreatitis,[46,47] and various types of injuries.[48–51] These diseases can be grouped into two categories, that is, mitochondrial oxidative stress (diabetes mellitus and cancer) and inflammatory oxidative conditions (i.e., atherosclerosis and ischemia). The important role of oxygen radicals in some human diseases is elaborated as follows.

2.3.1 | Cancer

Cancer is the leading cause of human death and is responsible for the most public health problems worldwide.[52] Its development is a complex process mediated by genetic, chemical, physical, and physiological factors. Specifically, chemical, physical, and physiological processes are closely associated with free radicals, which can readily induce DNA damage and oncogene activation. Moreover, due to loss of tumor suppressors, cancer cells have higher levels of ROS than normal cells.[53] Excessive reactive species alter growth signals and gene expression, and facilitate continuous proliferation of cancer cells. In prostate cancer cells, $O_2^{\bullet-}$ generated via a growth-regulatory NADPH oxidase exerts a cancer-promotion effect by providing a trophic intracellular oxidant tone to retard programed cell death.[54] $O_2^{\bullet-}$ produced via the adenosine triphosphate (ATP) pathway traps chemical carcinogens in the breast fluid, finally leading to fibroblasts proliferation, hyperplasia of epithelium, cellular atypia, and breast cancer.[55] Various lines of evidences have reported an elevated oxidative stress in patients with lung and bladder cancer,[56,57] and oxygen radicals can promote cell transformation into the malignant form with carcinoma as an endpoint.

2.3.2 | Neurodegenerative diseases

The high consumption of oxygen, the high content of oxidizable substrates (especially polyunsaturated fatty acid),[58] and the low level of antioxidant enzymes and species make the brain particularly susceptible to these oxidants.[59,60] For example, lipid peroxidation reduces the membrane fluidity and increases the membrane permeability to ions like Ca^{2+}, which is responsible for the neuron degradation in the central nervous system.[61] The oxidative stress has been involved in several neurodegenerative diseases such as AD,[62] PD,[63] Huntington's disease,[64] and multiple sclerosis.[65]

AD is characterized by extracellular neurotic plaques, intracellular neurofibrillary tangles, and deficient basal forebrain cholinergic neurons.[66] The neurotic plaque is made up of improper deposition of β-amyloid (Aβ) proteins while the neurofibrillary tangle is formed via the aggregation of hyperphosphorylated tau protein with Fe^{3+}. The Cu^{2+}-chelated Aβ protein can produce H_2O_2 in the presence of transition metal ions and further generate •OH.[67] Behl et al. have shown that Aβ aggregates interact with the neuronal membrane leading to cell apoptosis through the oxidation of membrane lipids' unsaturated carbohydrate side chains. Several markers of oxidative damages to lipids, proteins, and DNAs have been commonly found in AD brains. For example, an increased level of 8-OHdG in postmortem brain tissues was observed from AD patients compared with the control group. A high concentration of 4-HNE was detected in the amygdala and hippocampus regions from AD donors, which is toxic to neurons by altering their microtubule structure.[68,69]

PD is characterized by dopamine depletion especially in substantia nigra. Patients with PD show the elevated amount of oxidized lipids and proteins as a result of the redox imbalance.[70,71] The pathogenesis of PD is still unclear, but much attention is paid to the role of dopamine oxidation and the accelerated metabolism of dopamine. The latter may induce the excessive production of $O_2^{\bullet-}$, H_2O_2, and •OH, resulting in lipid peroxidation, membrane injury, and cell lysis.[72] As in AD patients, a marked enhancement in 4-HNE and 8-OHdG levels was also observed in PD brain regions.[73,74]

2.3.3 | Cardiovascular diseases

CVD refer to a class of eptiologies involving in the heart and blood vessels, coming from a variety of risk factors including hypertension, hypercholesterolemia, diabetes, smoking, and poor diet.[75] In recent years, it has become increasingly clear that abnormal formation of oxygen free radicals contributes to the initiation, progression, and development of a number of CVD such as atherosclerosis and ischemia.[76–78]

2.3.4 | Rheumatoid arthritis

RA is an autoimmune inflammatory disease characterized by an irreversible joint disorder such as joint swelling, joint deformity, and destruction of articular tissues.[79] Several lines of evidences indicate that over-produced free radicals account for the inflammation and destruction in the joints of both arthritic animals and RA patients.[80–82] Diverse pro-inflammatory mediators, such as macrophages and neutrophils, are activated to drive T-lymphocytes into affected joints and release pro-inflammatory cytokines for characteristic changes in RA.
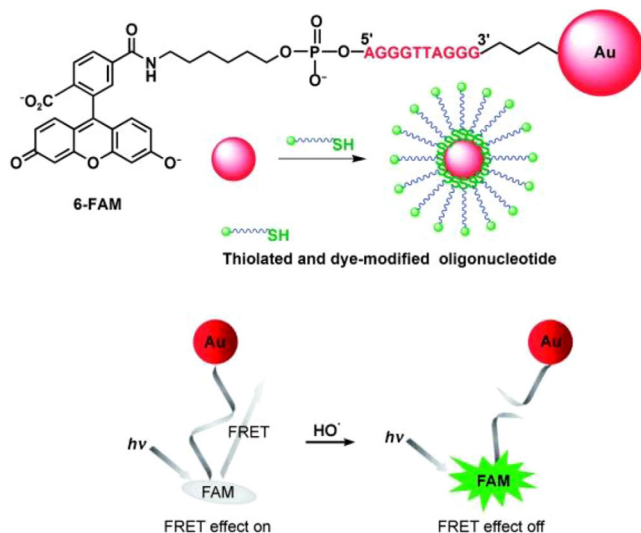
FIGURE 1 Chemical structure of FAM-DNA-AuNP and the FRET-based response mechanism of nanoprobe for •OH detection *Source*: Reprinted with permission from Wiley.[83]

3 | RESPONSIVE NANOPROBES FOR HYDROXYL RADICAL

Responsive luminescent nanoprobes for hydroxyl radical (•OH) detection have been designed by exploiting the oxidation of •OH with (i) DNA; (ii) fluorescent nanocrystals, including gold nanoclusters (AuNCs), silver nanoclusters (AgNCs), and silicon quantum dots (Si QDs); and (iii) fluorescent nanoparticles' surface dyes such as coumarin, cyanine derivatives, and azo dyes. In the following sections, the design of responsive nanoprobes, the performance of these nanoprobes in detecting •OH, and their biological applications are summarized.

3.1 | Oxidation and cleavage of DNA

The first example of DNA oxidation and cleavage-based responsive nanoprobe for •OH was reported by Tang's group in 2008 (Figure 1).[83] The thiol group at 3′-termini-functionalized single-stranded DNA (ssDNA) was first labeled with 6-carboxyfluorescein (6-FAM) at 5′-termini. The nanoprobe was then fabricated through binding DNA's thiol group (–SH) to 15 nm gold nanoparticles (AuNPs). Emission of 6-FAM was quenched due to the Förster resonance energy transfer (FRET) to nonemissive AuNPs. In the presence of •OH, oxidation cleavage of the DNA chain led to the release of 6-FAM and an increased emission at 517 nm (λ_{ex} = 490 nm). This nanoprobe showed high selectivity and sensitivity (limit of detection, LoD 2.4 nM), and fast response (<15 min), which allowed the nanoprobe for imaging of •OH in living macrophages and HepG2 cells. Through attaching 6-FAM-

labeled DNA-SH and pegylated galactose (PEG-Gal)-SH on the surface of AuNPs, a similar nanoprobe was then developed by Ma et al. in 2018.[84] This Gal-mediated hepatocyte-targetable nanoprobe was then applied to investigate the •OH production in acetaminophen or triptolide-induced liver injury.

In 2019, Zhou et al. reported a new signal amplification concept named as cytoplasmic protein-powered in situ fluorescence amplification (CPFA), and then proved the concept in the development of a responsive nanoprobe for •OH detection (Figure 2).[85] In this nanoprobe, the PBF1 fluorophore was entrapped inside mesoporous silica nanocontainer (MSN) with an ssDNA/PTAD-based gatekeeper. Upon reacting with •OH in living cells, the ssDNA was cleaved to separate perylene tetracarboxylic acid diimidedimmer, a cationic perylene derivative (PTAD) from MSN. Then, PBF1 was released to switch on the fluorescence. Interestingly, the released PDF1 in living cells can immediately bind with cytoplasmic proteins to further amplify the emission signal. As a result, about 400-fold enhancement in fluorescence at 620 nm was observed within several seconds. An extremely low LoD (6.4 pM) was thus obtained for this CPFA approach. Then, the nanoprobe was successfully applied for •OH analysis in RAW264.7 macrophages, HL-7702 and HepG2 cells.

3.2 | Oxidation of nanocrystals

In 2013, Chen et al. reported the first example of AuNC-decorated silica nanoparticles for ratiometric fluorescence detection of hROS (Figure 3).[86] AuNCs, prepared using a glutathione (GSH) template, were conjugated with biotinylated cell penetration peptide and then bond to streptavidin-functionalized silica nanoparticles (CF405S@SiNP). Under excitation at 405 nm, the nanoprobe showed dual emissions at 435 nm (CF405S) and 565 nm (AuNCs). In the presence of hROS, AuNCs' emission was quenched while CF405S's emission was retained. In comparison with HOCl and ONOO⁻, oxidation with •OH showed a greater change of the relative emission intensity (I_{435}/I_{565}). Despite high sensitivity to •OH (LoD 30 nM), selective detection of •OH is not possible using this nanoprobe. In 2014, Zhang et al. reported a DNA-templated AgNCs (DNA-AgNCs) for •OH detection.[87] DNA-AgNCs showed green emission at 550 nm, while the emission was quenched after reacting with •OH. The emission quench is attributed to the aggregation of AgNCs after cleavage of DNA template. The selectivity of DNA-AgNCs to other hROS (HOCl and ONOO⁻) was not evaluated, although this nanoprobe was highly selective to some ions and amino acids.

Fluorescent Si QDs were also found to be sensitive to ROS.[88] Based on this response mechanism, Zhao
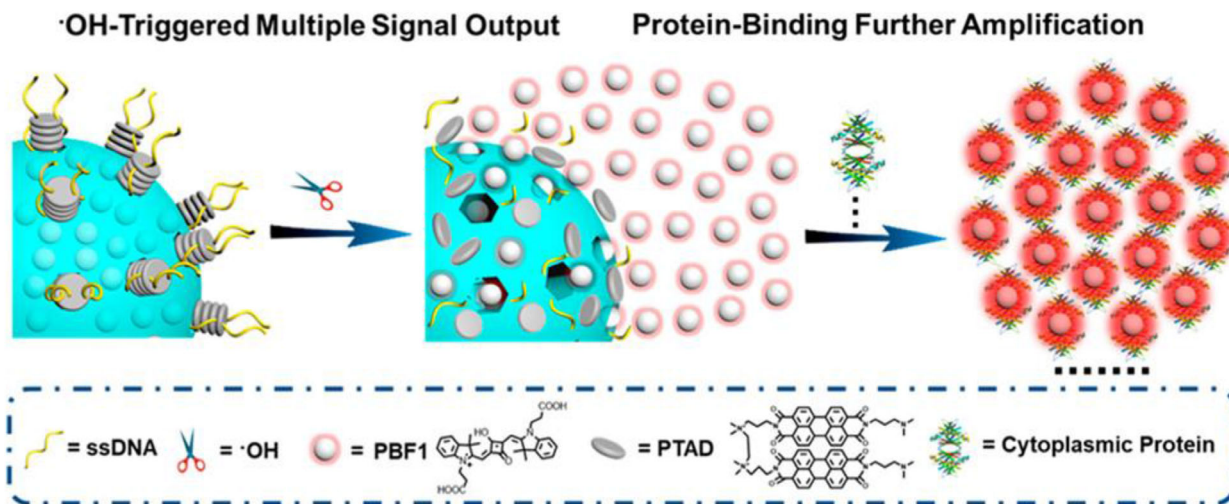
FIGURE 2 Response mechanism of cytoplasmic protein binding based CPFA nanoprobe for •OH and its two-stage amplification process
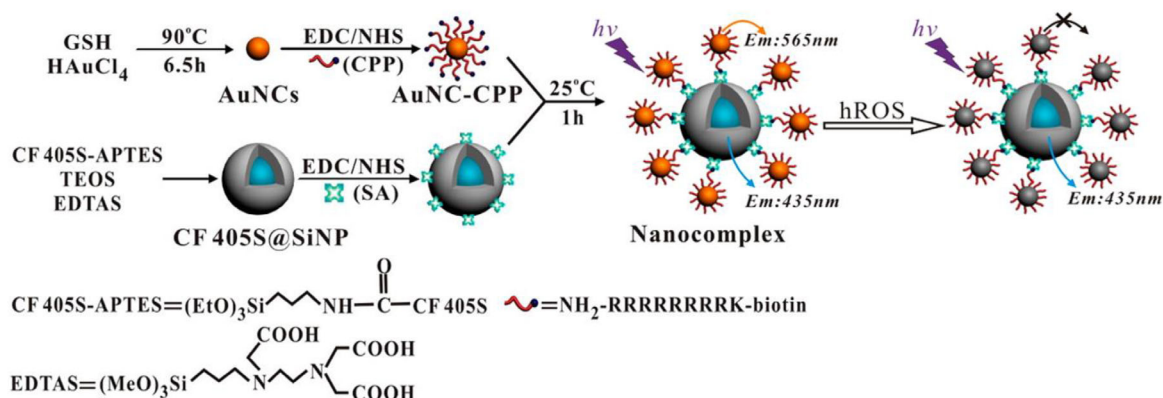*Source*: Reprinted with permission from American Chemical Society

FIGURE 3 Preparation of the AuNC-coated CF405S@SiNP and its response mechanism for •OH detection
Source: Reprinted with permission from American Chemical Society.[86]

et al. reported chlorin e6 (Ce6)-conjugated Si QDs as the nanoprobe (Si-Ce6 QDs) for ratiometric fluorescence detection of •OH.[89] Upon reacting with •OH, the emission of Si-Ce6 QDs at 490 nm was quenched while that at 660 nm retained, which allowed Si-Ce6 QDs for ratiometric fluorescence (I_{660}/I_{490}) detection of •OH in buffer solutions and in living HepG2 cells. Results of selectivity experiments showed that nanoprobe is able to selectively detect •OH with limited interference from HOCl and ONOO⁻.

3.3 | Hydroxylation of coumarin and terephthalic acid

Coumarin-3-carboxylic acid (CCA) is a nonfluorescent dye that can specifically react with •OH to form emissive 7-hydroxy-CCA (7-OH-CCA) (Scheme 2A).[90] As a result of hydroxylation of coumarin, the intramolecular charge transfer (ICT) based fluorescence is switched on and the change of the emission intensity is corresponding to the concentration of •OH. Based on this response mechanism, several responsive nanoprobes were developed for ratiometric fluorescence detection of •OH.[91] These nanoprobes were normally designed by conjugating CCA on the surface of fluorescent nanoparticles.[92,93] Similar to CCA, nonfluorescent terephthalic acid (TPA) can also react with •OH specifically to form the fluorescent product, 2-hydroxyl terephthalic acid (hTPA) (Scheme 2B).[94] Thus, TPA was used as a favorable fluorescent radical trapping agent for high-performance liquid chromatography analysis.
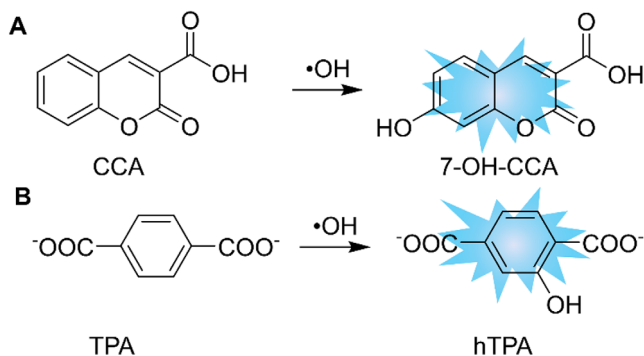
SCHEME 2 Reaction of CCA, TPA with •OH to produce fluorescent 7-OH-CCA (A), hTPA (B), respectively

In 2011, Ganea et al. reported a coumarin-neutral red (CONER) nanoprobe for •OH detection.[92] The CONER was developed using biocompatible poly(lactide-co-glycolide) nanoparticles to encapsulate neutral red as the reference dye and CCA-conjugated poly(sodium N-undecylenyl-Ne-lysinate) as the •OH recognition unit. Encapsulating neutral red in the polymeric matrix minimized its side reactions with other reactive species. Hydroxylation reaction between CCA and •OH led to the formation of fluorescent 7-OH-CCA, followed by the FRET from 7-OH-CCA to neutral red. The ratiometric change of emissions (I_{450}/I_{528}) showed good selectivity and sensitivity (LoD 0.73 μM) for •OH detection and imaging in MCF-7 cells. Through conjugating CCA to the amino-functionalized carbon nanodots (CDs), CCA@TPP@CDs nanoprobe was recently developed by Zhou et al. for •OH detection.[93] In the presence of •OH, CCA emission was increased remarkably while CDs emission remained constant. The ratiometric change of blue (420–500 nm) and yellow (530–610 nm) emissions showed a good linearity with the concentration of •OH in the range of 0.1–160 mM with a LoD 70 nM. The conjugation of triphenylphosphonium bromide (TPP) facilitated the accumulation of CCA@TPP@CDs to the mitochondria, which allowed for the imaging of •OH production in RAW264.7 cells at a subcellular level.

Nanoscale graphene QDs (GQDs) have been widely used in the development of nanoprobes for bioassay and imaging due to their excellent solubility, low toxicity, and favorable biocompatibility. Conjugating TPA onto the surface of GQDs through π–π interactions, Hai et al. developed nanoprobe (TPA@GQDs) for sensitive assay and quantification of •OH in aqueous solutions and living cells.[95] In the presence of •OH at 0.018-6 μM, the nanoprobe emission was greatly increased. TPA@GQDs had high sensitivity (LoD 12 nM) and selectivity to •OH detection, allowing for •OH quantification in lake water samples and imaging in living HeLa cells.

3.4 | Production, oxidation, and cleavage of C=C bond

Another GQDs-based nanoprobe (GQD-hydroIR783) for •OH detection was demonstrated by Liu et al. in 2018.[96] The GQD-hydroIR783 nanoprobe was developed in a similar way to fabrication of TPA@GQDs, where the hydroIR783 dyes were conjugated to GQDs through π–π staking. Different from TPA@GQDs, GQD-hydroIR783 showed bright yellow emission at 520 nm. In the presence of •OH and $O_2^{\bullet-}$, oxidation of hydroIR783 occurred to produce IR783, accompanied by a significant increase in absorbance and fluorescence. The FRET from GQDs to IR783 was also obtained, allowing for ratiometric fluorescence (I_{800}/I_{520}) analysis of •OH and $O_2^{\bullet-}$ under excitation at 440 nm. Although GQD-hydroIR783 could not discriminate •OH and $O_2^{\bullet-}$, imaging of both oxygen radicals in RAW 264.7 cells and lipopolysaccharide (LPS) stimulated inflammation in mice were successfully demonstrated.

It has been reported that the electron deficit C=C bond is not stable in the presence of hROS.[97] This C=C bond is able to react with •OH, HOCl, and ONOO⁻ through oxidation and cleavage reactions.[98] As a result, a few small molecule based responsive probes have been developed for •OH, HOCl, and ONOO⁻ detection.[9,99,100] In 2018, Cong et al. reported a nanoGUMBOS (a group of uniform materials based on organic salts) as the nanoprobe specific for •OH detection.[101] This nanoGUMBOS nanoprobe was developed by self-assembling 1,1′-diethyl-2,2′-cyanine bis(trifluoromethanesulfonyl)imide ([PIC][NTf$_2$]) and 1,1′-diethyl2,2′-carbocyanine bis(trifluoromethanesulfonyl)imide ([PC][NTf$_2$]). In the presence of •OH, emission of nanoGUMBOS at 662 nm was decreased while that at 589 nm remained constant. This [PIC-PC][NTf$_2$] binary nanoprobe exhibited a LoD (700 nM) and relatively high selectivity in ratiometric fluorescence detection of •OH.

Upconversion nanoparticles (UCNPs) that can convert low-energy photons to high-energy emissions are gaining increasing interests in recent biomedical research.[102–104] To develop UCNPs-based responsive nanoprobes, small molecules that are responsive to analyte are normally attached to the surface of UCNPs. The emission of UCNPs is then regulated by the FRET from UCNPs to small molecules.[104] Through attaching indocyanine green (ICG) to oleic acid removed UCNPs (NaLuF$_4$:Yb,Er), UCNP-ICG was developed by Guo et al. for •OH detection (Figure 4).[105] In the presence of •OH, oxidation and cleavage of the C=C bond in ICG led to the blue shift of absorption spectra. As a result, FRET from NaLuF$_4$:Yb,Er's emission at 654 nm to ICG was abolished, while a new FRET process from NaLuF$_4$:Yb,Er's emission at 540 nm
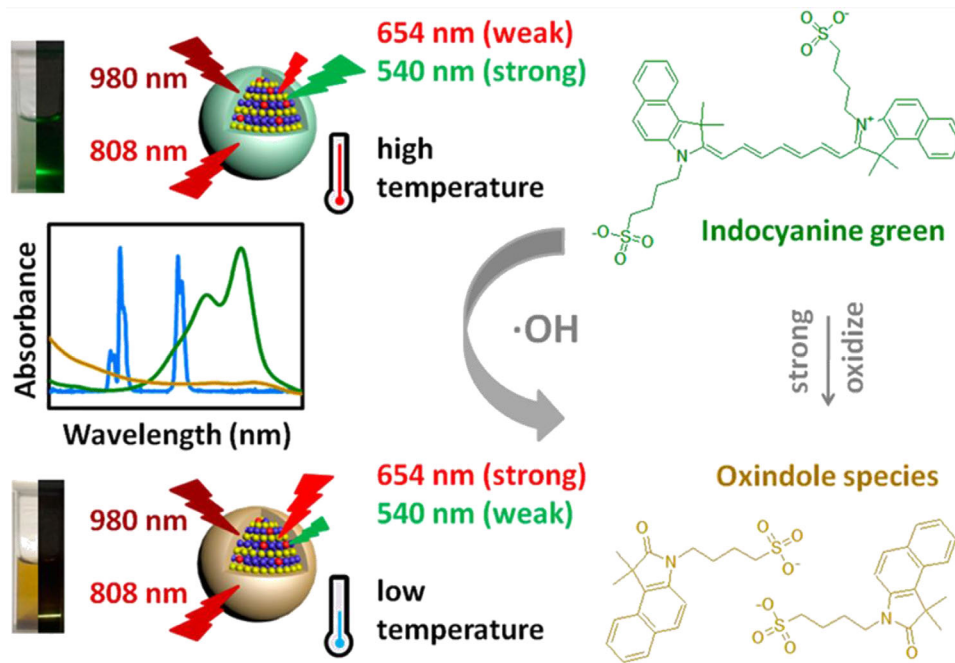
FIGURE 4 Design of the UCNP-ICG, the FRET process, and the response mechanism for •OH detection
Source: Reprinted with permission from American Chemical Society.[105]

to the oxidation product emerged. Upconversion luminescence (UCL) at 654 nm thus increased while that at 540 nm decreased, allowing UCNP-ICG for ratiometric luminescence (I_{654}/I_{540}) detection of •OH in the range of 250 nM to 2 μM with a very low LoD ($\sim$4 pM). Tm-doped UCNPs are featured with near-infrared (NIR) emission at 812 nm. Attaching IR-808 dyes to the surface of NaGdF$_4$:Yb,Tm@NaYF$_4$ core–shell UCNPs, Zhao et al. developed UCNPs-IR-808 nanoprobe for •OH detection produced in the Fe^{2+}–H$_2$O$_2$ system.[106] NIR emission of UCNPs-IR-808 was increased upon reacting with the Fe^{2+}–H$_2$O$_2$ system, attributed to the destruction of FRET from UCNPs to IR-808 after the •OH-mediated cleavage of IR-808′s C=C bond.

3.5 | Oxidation and decomposition of azo dye

Through attaching modified Orange G, an azo dye (mOG) on the surface of UCNPs (NaYF$_4$@NaYF$_4$:Yb,Tm@NaYF$_4$), Li et al. reported a UCL nanoprobe (mOG-SWUCNPs) for •OH detection (Figure 5).[107] mOG-SWUCNPs were composed of two moieties, that is, UCNPs with blue emission as the energy donor, and mOG azo dye with tuneable absorption as both energy acceptor and the •OH recognition unit (Figure 5A). The blue UCL was quenched due to the FRET to

mOG. In the presence of •OH, the azo bond (N=N) was oxidized and then decomposed, resulting in a decrease in mOG's absorbance at 487 nm. The blue UCL was then increased due to the destruction of FRET (Figure 5B). The blue UCL increment showed a linear relationship with the •OH concentration from 1.2 to 194.6 fM, resulting in an extremely low quantification limit (1.2 fM) using mOG-UCNPs nanoprobe. This probe was then applied to investigate the •OH production in HeLa cells (Figure 5C) and in liver tissues of LPS-treated mice (Figure 5D).

Using core–multishell (CMS)-UCNPs (NaYF$_4$@NaYF$_4$:Yb,Tm@NaYF$_4$:Yb,Er@NaYF$_4$) as the energy donor and an azo dye (2-hydroxy-1-(2-hydroxy-4-sulfo-1-naphthylazo)-3-naphthoic acid) as the energy acceptor, Song et al. prepared a CMS-UCNPs@azo dye nanoprobe for •OH detection in 2017.[108] Green UCL at 545 nm was quenched (97% quenching yield) due to the FRET to azo dye. In the presence of •OH, the azo N=N bond was oxidized and then cleaved, leading to the enhancement of green UCL. The increment of UCL intensity at 545 nm showed a linear relationship with the •OH concentration (0.10−163.20 fM), and the quantification limit was 0.1 fM, more than 10 times lower than that of mOG-UCNPs nanoprobe.[107] The CMS-UCNPs@azo dye nanoprobe was then applied to successfully image •OH in HeLa cells, liver tissues of LPS-stimulated mice, and tumor tissues of the tumor-bearing mice.
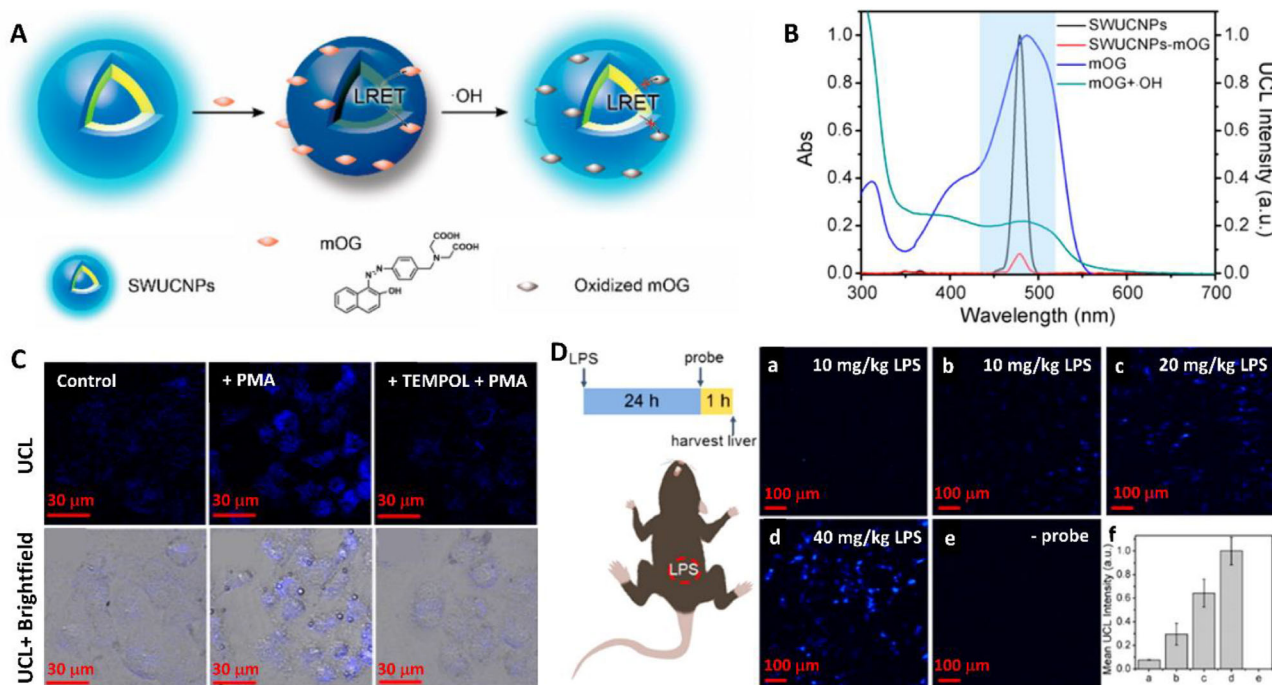
FIGURE 5 mOG-SWUCNPs nanoprobe for •OH detection and UCL imaging

Note: Design of mOG-SWUCNPs for •OH detection (A) UCL emission and mOG absorption in the absence and presence of •OH (B) UCL images of HeLa cells treated with PMA (500 ng/mL), TEMPOL (radical scavenger), and then stained with mOG-SWUCNPs (0.3 mg/mL) (C) UCL images of mouse liver slice treated with LPS and mOG-SWUCNPs (30 mg/kg, body weight) (D)

Source: Reprinted with permission from American Chemical Society.[107]

3.6 | Oxidation of other organic dyes

Nonfluorescent methylene blue (MB) has intense absorption around 650 nm. This dye can be readily oxidized to unstable smaller organic byproducts and then decomposed to smaller inorganic species, such as H_2O, Cl^-, CO_2, and SO_4^{2-} in the presence of •OH and other free radicals.[109] Based on this oxidation-degradation mechanism, Yu et al. reported an MB-UCNPs@PSS nanoprobe for •OH detection (PSS: sodium polystyrene sulfonate).[110] The nanoprobe was developed by coating positively charged MB on the negatively charged UCNPs@PSS. Red UCL of $NaGdF_4$:Yb,Er@$NaGdF_4$ was quenched due to the energy transfer to MB. In the presence of •OH, oxidation degradation of MB led to the decrease in MB's absorption at 654 nm, and thus the recovery of red UCL. This nanoprobe showed high selectivity and sensitivity (LoD, 2 nM) for •OH detection in vitro. UCL imaging of •OH in HeLa cells and liver tissues of LPS-stimulated mice was also demonstrated. In another UCNPs-based nanoprobe for •OH detection, lysine-functionalized $NaYF4$:Yb,Er was conjugated with carminic acid (CA) through an amide bond.[111] The green UCL of CA-UCNPs was quenched due to the FRET to CA, while it was recovered after •OH-

mediated oxidative cleavage of CA. The CA-UCNPs was then used for evaluating the antioxidant activities of five traditional Chinese medicines.

To monitor the oxidative stress-induced •OH production in living organisms, reversible probes are more preferable because the probes can be recycled in-situ in living organisms after the detection.[112] Most of the UCNPs-based nanoprobes are irreversible, and have to be disposed after detection each time. To address this issue, Liu et al. reported a reversible UCNPs nanoprobe for •OH detection (Figure 6).[113] The probe was developed by exploiting the response mechanism of oxidation-reduction of 4-amino salicylic acid-iron(II) complex (4-ASA-Fe(II)). As the reversible change between 4-ASA-Fe(II) and 4-ASA-Fe(III) occurred in the range of 400–600 nm in absorption spectra, both green and red UCL of $NaLuF_4$:Yb,Er,Tm were switched off. This nanoprobe had a broad linear range (4 nM to 16 mM) with a low LoD (~2 nM). Detection and imaging of nano-TiO_2-induced oxidative stress were then demonstrated in vitro and in vivo.

Oxidative cleavage of hydroquinone ether derivatives, such as 2-[6-(4′-hydroxy)phenoxy-3H-xanthen-3-on-9-yl]benzoic acid (HPF) and derivatives, has been widely used in the design of •OH responsive molecular
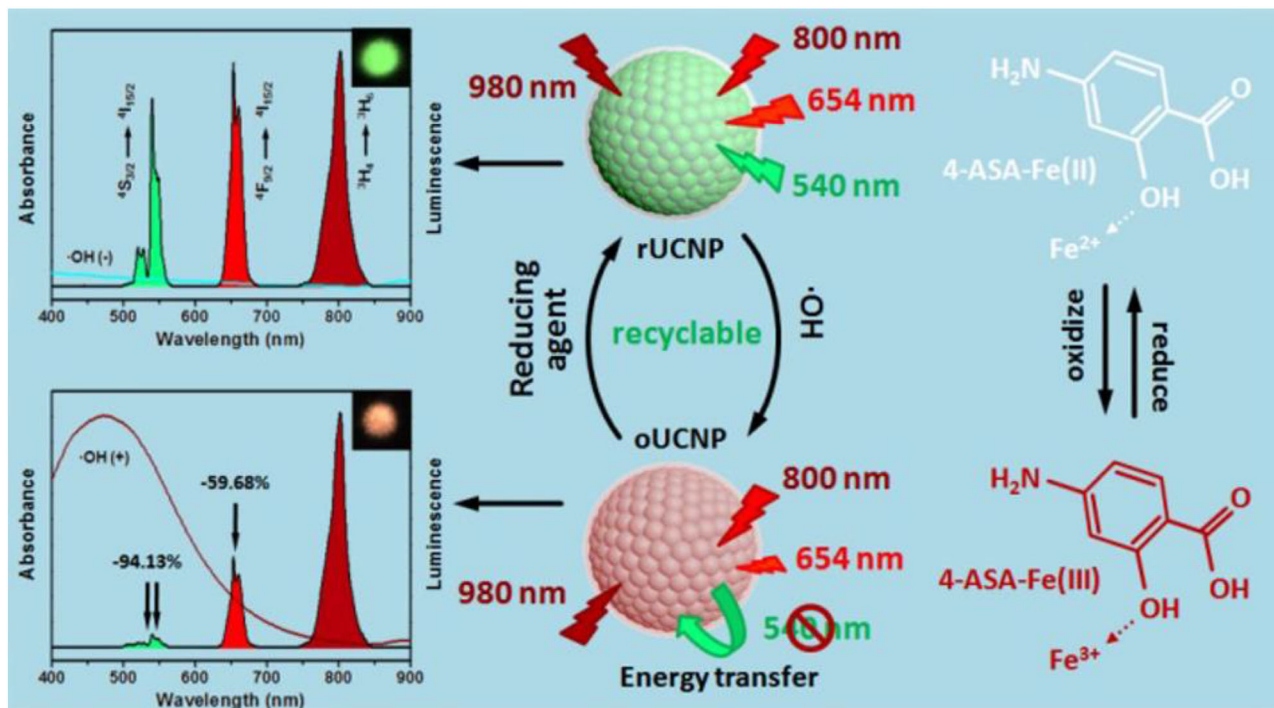
FIGURE 6 Design of the ratiometric UCL nanoprobe for •OH detection based on reversible oxidation-reduction of 4-ASA-Fe(II)
Source: Reprinted with permission from American Chemical Society.[113]

probes.[114,115] Conjugating these molecules to fluorescent nanoparticles, ratiometric probes for fluorescent detection of •OH were then developed.[116] For example, Zhuang et al. reported an AuNC@HPF probe for •OH detection in PBS buffer and living cells.[117] AuNC@HPF probe was developed by conjugating HPF to bovine serum albumin (BSA) protected AuNCs. BSA-AuNCs showed red emission at 637 nm in PBS buffer. Due to oxidation cleavage of ether bond to produce fluorescein, green emission at 515 nm emerged and increased according to the concentration of •OH. AuNC@HPF probe was then used for ratiometric fluorescence imaging of •OH production in LPS-stimulated HeLa cells.

4 | RESPONSIVE NANOPROBES FOR SUPEROXIDE ANION

The responsive mechanism for designing nanoprobes for $O_2^{\bullet-}$ detection mainly involves oxidation of (i) fluorescent nanodots (NDs) such as Au ND (Au ND), Ag nanoparticles (AgNPs), and CdTe QDs; (ii) guanine to hydroxyguanine; and (iii) organic dyes such as hydroethidine (HE) and 2-chloro-1,3-dibenzothiazolinecyclohexene (DBZTC). In this section, progresses in the development of responsive nanoprobes for $O_2^{\bullet-}$ detection are discussed according to the response mechanisms and nanomaterials.

4.1 | Oxidation of fluorescent nanodots

Au NDs, prepared by a one-pot approach using D(+)-mannose as the reducing agent and 2-mercaptobenzothiazole as the stabilizing agent, were developed by Li et al. for $O_2^{\bullet-}$ detection and cell imaging.[118] This nanoprobe showed intense orange fluorescence (λ_{em} = 532 nm), while this emission was quenched in the presence of $O_2^{\bullet-}$. The quenching of Au ND's emission was attributed to the oxidation of Au into Au(I) after reaction with $O_2^{\bullet-}$. The oxidation of Au NDs showed good selectivity to $O_2^{\bullet-}$ over other ROS, metal ions, and amino acids. In addition, Ag NCs have outstanding nonenzymatic catalytic performance for $O_2^{\bullet-}$ reduction.[119,120] Based on this response mechanism, Liang et al. reported a CD@Ag NCs core–shell structured nanoprobe for $O_2^{\bullet-}$ detection and cell imaging.[121] In this nanoprobe, CDs were first prepared and then coated with Ag NCs to form CD@Ag NCs. As a result of Ag NC coating, emission of CDs at 440 nm was quenched, but switched on in the presence of $O_2^{\bullet-}$. The "off-on" fluorescence response was attributed to the release of fluorescent CD after $O_2^{\bullet-}$-mediated etching of Ag NCs.

Through modulating the space and distance between surface molecules and QDs, two QD-based nanoprobes were developed for $O_2^{\bullet-}$ detection. As reported by Adegoke et al., thiol-capped CdTe@ZnS QDs were conjugated
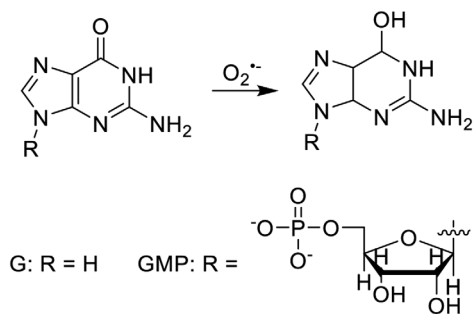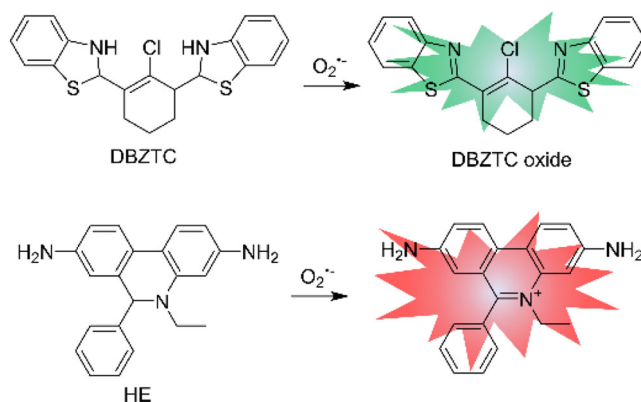
SCHEME 3   Response mechanism of G and GMP with $O_2^{\bullet-}$

SCHEME 4   Chemical structures of DBZTC and HE and their response mechanisms with $O_2^{\bullet-}$

with cobalt tetraamino-phthalocyanine (CoTAPc).[122] In the presence of $O_2^{\bullet-}$, the emission of MPA-CdTe@ZnS-CoTAPc was gradually enhanced with the increasing concentration of $O_2^{\bullet-}$. This nanoprobe showed good selectivity and high sensitivity (LoD, 2.1-2.4 nM, depending on the size of QDs). In a later study, Han et al. prepared a CdTe QDs-Schiff base nanoprobe for $O_2^{\bullet-}$ detection.[123] In this nanoprobe, the emission of QDs was attenuated through conjugating Schiff base onto the surface. Upon reacting with $O_2^{\bullet-}$, the space and distance between the Schiff base and QDs were increased, resulting in enhancement of QDs' emission at 610 nm.

4.2 | Oxidation of guanosine-terbium (Tb) coordination polymer

Guanine (G) is one of the four bases in nucleic acids (DNA and RNA). This base can coordinate with Tb(III) to form the luminescent coordination polymer. In this coordination polymer, G severs as the antenna, in which the energy from G's triplet excited state transfers to Tb.[124] Green emission at about 545 nm of the G-Tb coordination polymer is thus generated from the sensitized Tb(III). In the presence of $O_2^{\bullet-}$, G reacting with $O_2^{\bullet-}$ leads to the formation of hydroxylated G (Scheme 3). The triplet excited state of hydroxylated G is inhibited and sensitization to Tb is thus blocked. Based on this response mechanism, several coordination polymers have been reported for $O_2^{\bullet-}$ detection.

In 2017, Song et al. reported a response nanoprobe (PS-SO₃H@Tb/G NCPs) for ratiometric luminescence detection of $O_2^{\bullet-}$ with high sensitivity and selectivity.[125] The PS-SO₃H@Tb/G NCPs was prepared using suffocated polystyrene nanoparticles as the core and Tb-G coordination polymer as the $O_2^{\bullet-}$ responsive shell. In the presence of $O_2^{\bullet-}$, Tb-G's emission at 544 nm was significantly decreased while PS-SO₃H's emission at 483 nm was slightly weakened, allowing PS-SO₃H@Tb/G NCPs for ratiometric luminescence (I_{544}/I_{483}) detection of $O_2^{\bullet-}$ with a low LoD (3.4 nM). Guanosine 5′-monophosphate (GMP) can also

be employed as the antenna for Tb sensitization as well as $O_2^{\bullet-}$ recognition (Scheme 3). In 2019, Yang et al. reported an "on-off" luminescence nanoprobe (SiO₂@Tb/GMP NCPs) for $O_2^{\bullet-}$ detection.[126] The nanoprobe was developed by coating Tb-GMP coordination polymer onto the surface of carboxyl-functionalized silica nanoparticles. In the presence of $O_2^{\bullet-}$, the green emission of Tb was quenched due to G hydroxylation. SiO₂@Tb/GMP NCPs showed a lower LoD (2.18 nM) than PS-SO₃H@Tb/G NCPs.

Using BSA-stabilized AuNPs (AuNPs-BSA) as the reference fluorophore, Liu et al. reported a nanoprobe for ratiometric luminescence detection of $O_2^{\bullet-}$.[127] This nanoprobe (AuNPs-BSA@Tb/GMP NCPs) was developed by coating Tb/GMP coordination polymer onto fluorescent AuNPs-BSA@Tb nanoparticles. The emission of AuNPs-BSA@Tb/GMP NCPs (I_{544}/I_{410}) was stable over 30 days during incubation in 50 mM of Tris-HCl buffer of pH 7. In the presence of $O_2^{\bullet-}$, the emission of Tb/GMP was significantly quenched while that of AuNPs-BSA was maintained, allowing for ratiometric luminescence detection of $O_2^{\bullet-}$ as well. This nanoprobe also showed high sensitivity (LoD 4.7 nM) and selectivity for $O_2^{\bullet-}$ detection.

4.3 | Oxidation of DBZTC

In 2007, Gao et al. found that DBZTC can be oxidized specifically by $O_2^{\bullet-}$ in Hepes buffer of pH 7.4 (Scheme 4).[128] The extended π-conjugation system of oxidized DBZTC shows intense green emission at 559 nm. On the basis of this response mechanism, Li et al. developed a metallic colloid-enhanced fluorescence silica nanoparticle for $O_2^{\bullet-}$ detection in 2012.[129] In this nanoprobe (DBZTC/Ag@SiO₂), AgNPs within the SiO₂ shell contributed to enhancing the fluorescence signals through surface plasmon resonance and DBZTC conjugated onto the surface of SiO₂ served as the $O_2^{\bullet-}$ recognition moiety.
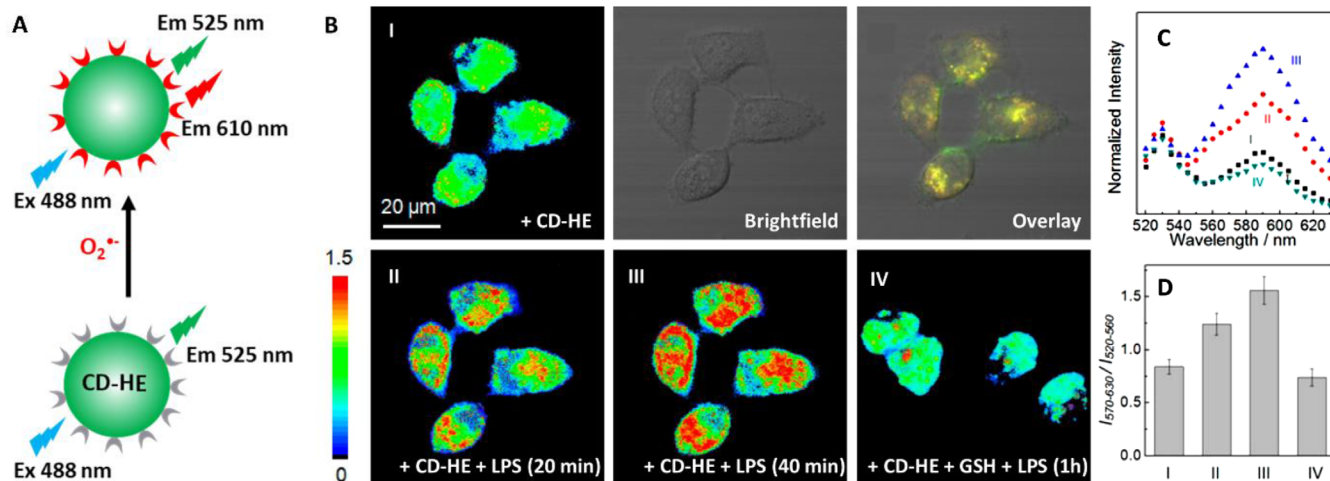
FIGURE 7 Design of ratiometric fluorescent CD-HE nanoprobe for $O_2^{\bullet-}$ (A) Ratiometric fluorescence imaging of HeLa cells stained with CD-HE before and after treatment with LPS and GSH + LPS (B) Intracellular fluorescence spectra (C) and ratiometric intensities (D) of HeLa cells under different treatment in (B)
Source: Reprinted with permission from American Chemical Society.[131]

In the presence of $O_2^{\bullet-}$, oxidation of DBZTC in 20 mM Hepes buffer of pH 7.4 resulted in remarkable enhancement of green emission. DBZTC/Ag@SiO$_2$ exhibited high sensitivity (LoD 0.73 nM) and selectivity (1000-fold higher sensitivity than that to H_2O_2), allowing for imaging of $O_2^{\bullet-}$ production in RAW 264.7 cells.

In a later study, the same group loaded DBZTC and another pH-responsive dye (Tpy-Cy) into rhodamine b (RhB)-encapsulated MSN nanoparticles.[130] The prepared nanoprobe (DBZTC@Tpy-Cy@CS) showed dual ratiometric fluorescence responses to $O_2^{\bullet-}$ and pH in buffered solutions and living cells. RhB's emission at 575 nm was maintained but DBZTC's emission at 527 nm was increased with the increasing concentration of $O_2^{\bullet-}$. Conjugating TPP on the surface of DBZTC@Tpy-Cy@CS allowed it to accumulate in mitochondria after internalization. Therefore, changes of the $O_2^{\bullet-}$ level in mitochondria of HeLa cells during autophagy and apoptosis processes were monitored using DBZTC@Tpy-Cy@CS. The results showed that the $O_2^{\bullet-}$ level was increased at the early stage of apoptosis and almost constant at the initial stage of autophagy.

4.4 | Oxidation of HE

Similar to DBZTC and hydroIR783,[96] oxidation of HE has also been exploited as the response mechanism for the development of nanoprobes for $O_2^{\bullet-}$ detection (Scheme 4). The oxidation product has an extended π-conjugation, showing intense red emission at 610 nm. Through conjugating HE onto the surface of CDs, Gao et al. developed a responsive nanoprobe (CD-HE) for ratiometric

fluorescence detection of $O_2^{\bullet-}$ (Figure 7).[131] Upon excitation at 488 nm, CDs' emission at 525 nm was maintained while HE's emission at 610 nm increased with the $O_2^{\bullet-}$ level (Figure 7A). Ratiometric fluorescence imaging of $O_2^{\bullet-}$ production in LPS- and GSH-treated HeLa cells showed that the $O_2^{\bullet-}$ level was increased over the time during LPS treatment, then recovered to the normal level after treatment with GSH for 30 min (Figure 7B). The corresponding intracellular fluorescence spectra (Figure 7C) and ratiometric intensities (Figure 7D) indicated the reliability of ratiometric detection of $O_2^{\bullet-}$. Using Qdot 800 ITK carboxyl CdSe/ZnS core–shell QDs (QD800) within SiO$_2$ nanoparticle as a reference signal, the same group then developed ratiometric fluorescence nanoprobe for the detection of $O_2^{\bullet-}$ and pH.[132] The nanoprobe (HE + FITC + TPP-SiO$_2$@QD) was further developed by conjugating FITC and HE to the surface of SiO$_2$@QD. HE's emission was switched on in the presence of $O_2^{\bullet-}$ and FITC's emission was modulated by the change of pH, while QDs emission was remained constant in all test conditions. This nanoprobe was then successfully applied for $O_2^{\bullet-}$ and pH imaging in mitochondria in living RAW264.7 macrophages.

Conjugating aminofluorescein (AF) and HE onto the surface of MSN, Pan et al. reported a ratiometric fluorescence nanoprobe for $O_2^{\bullet-}$ and pH detection in 10 mM PBS buffer and living cells.[133] Similarly, both green (AF) and red (HE) emissions were changed according to the pH and $O_2^{\bullet-}$ levels. Carboxyl-functionalized MSN surface allowed conjugation of TPP and MPP, which facilitated the accumulation of nanoprobe in mitochondria and lysosomes, respectively, after cellular internalization. This probe was
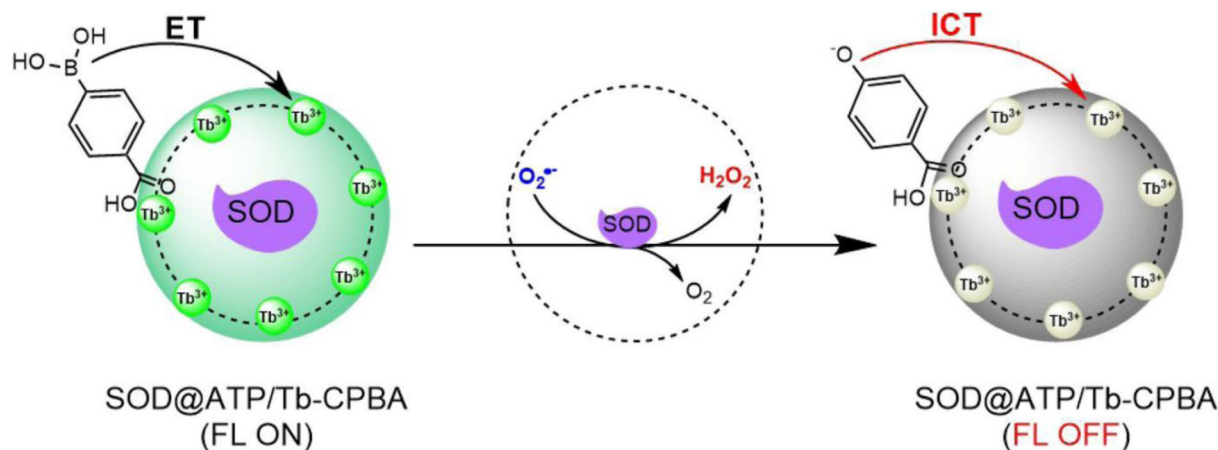
FIGURE 8 Response mechanism of SOD@ATP/Tb-CPBA to $O_2^{\bullet-}$
Source: Reprinted with permission from American Chemical Society.[138]

then used for subcellular imaging for the $O_2^{\bullet-}$ level change in MCF-7 cells. A similar nanoprobe for pH and $O_2^{\bullet-}$ detection and imaging in HeLa cells and LPS-stimulated mice was then developed on a DNA tetrahedron nanoparticle platform by the same research group.[134]

Loading HE onto MSN and $hmSiO_2$ is another approach for developing the responsive nanoprobe for $O_2^{\bullet-}$ detection. In 2018, Cheng et al. reported a nanoprobe for simultaneous detection of hydrogen selenide (H_2Se) and $O_2^{\bullet-}$ around mitochondria in HepG2 cells under hypoxic conditions.[135] In this nanoprobe (Mito-N-D-MSN), HE and another H_2Se-responsive dye (NIR-H_2Se) were loaded onto the MSN surface. The nanoparticles were then coated with PEI and conjugated with TPP, which allowed for detection and imaging of $O_2^{\bullet-}$ in mitochondria in HepG2 cells. In another work, HE was loaded onto $hmSiO_2$ NPs with an FITC-labeled $mSiO_2$ core.[136] Encapsulating FITC within $mSiO_2$ allowed the emission intensity of core nanoparticle stable, while HE on the $hmSiO_2$ NP surface was able to respond to and ratiometrically detect the $O_2^{\bullet-}$ level change. The nanoprobe displayed high sensitivity (LoD 80 nM) and selectivity to $O_2^{\bullet-}$ over other ROS and biologically relevant oxidants. Ratiometric fluorescence imaging and flow cytometry analysis of the $O_2^{\bullet-}$ level change in HeLa cells were then investigated.

4.5 | Oxidation of other dyes

Encapsulating rhodamine-B (RDB) within Schiff base polymer (SBP), Du et al. developed a dual emission nanoprobe (SBP/RDB) for ratiometric fluorescence detection of $O_2^{\bullet-}$.[137] Under excitation at 270 nm, SBP/RDB showed emissions of SBP at 485 nm and RDB at 585 nm. In the presence of $O_2^{\bullet-}$, the emission at 585 nm was quenched

while the emission at 485 nm was maintained constant. Quenching RDB's emission is attributed to oxidation and cleavage of C–O–C bond of RDB. The π-conjugation system of RDB is disrupted and the π–π interaction between SBP and RDB thus blocked. Very recently, a coordination polymer-based nanoprobe (SOD@ATP/Tb-CPBA, where CPBA is carboxyphenylboronic acid) was developed by Weng et al. for $O_2^{\bullet-}$ detection (Figure 8).[138] SOD@ATP/Tb-CPBA used Tb as an emitter, ATP as a bridge ligand, and CPBA as an antenna for Tb sensitization. SOD in this nanoprobe is able to covert $O_2^{\bullet-}$ to H_2O_2 that then reacts with CPBA through deboronation. The ICT process from hydroxybenzoic acid to Tb resulted in quenching of Tb emission in correspondence to the $O_2^{\bullet-}$ concentration. This nanoprobe showed high sensitivity (LoD 25 nM) and selectivity to $O_2^{\bullet-}$ over other ROS, potentiating the application in $O_2^{\bullet-}$ detection in serum samples.

5 | CONCLUSION AND OUTLOOK

This review article briefly summarizes the ODFR species and their detection by responsive nanoprobes. The production and biological properties of ODFRs were first introduced, followed by simply discussing the mechanisms of ODFRs in oxidation of nucleus acids, lipids, proteins, and carbohydrate, and their roles in diseases' development. Bioanalytical methods for $O_2^{\bullet-}$ and •OH detection, particularly the responsive nanoprobes for luminescent analysis of these two radicals were then summarized in detail (Table 1). Most of the nanoprobes showed high sensitivity for $O_2^{\bullet-}$ and •OH detection, with the LoD being at the nanomolarity level. UCNPs-based nanoprobes, such as UCNP-ICG, mOG-SWUCNPs, and UCNPs@azo dye were recently developed and showed a 10^3–10^6 time lower level

TABLE 1 Responsive nanoprobes for detection and bioimaging of $O_2^{\bullet-}$ and $\bullet OH$

Responsive nanoprobes	Radical	Samples for bioassay	Sensitivity (LoD/LoQ)	Reference
FAM-DNA-AuNPs	$\bullet OH$	Macrophages and HepG2 cells	2.4 nM (LoD)	83
MSN/ssDNA/PTAD	$\bullet OH$	RAW264.7 macrophages, HL-7702 and HepG2 cells	6.4 pM (LoD)	85
Si-Ce6 QDs	$\bullet OH$	HepG2 cells	/	89
CONER	$\bullet OH$	MCF-7 cells	0.73 μM (LoD)	92
CCA@TPP@CDs	$\bullet OH$	RAW264.7 cells	70 nM (LoD)	93
TPA@GQDs	$\bullet OH$	HeLa cells	12 nM (LoD)	95
UCNP-ICG	$\bullet OH$	/	4 pM (LoD)	105
mOG-SWUCNPs	$\bullet OH$	HeLa cells and liver tissues of LPS-treated mice	1.2 fM (LoQ)	107
(CMS)-UCNPs@azo dye	$\bullet OH$	HeLa cells, liver tissues of LPS-stimulated mice, and tumor tissues of the tumor-bearing mice	0.10 fM (LoQ)	108
UCNPs@PSS	$\bullet OH$	HeLa cells and liver tissues of LPS-stimulated mice	2 nM (LoD)	110
PS-SO$_3$H@Tb/G NCPs	$O_2^{\bullet-}$	/	3.4 nM (LoD)	125
SiO$_2$@Tb/GMP NCPs	$O_2^{\bullet-}$	/	2.18 nM (LoD)	126
DBZTC/Ag@SiO$_2$	$O_2^{\bullet-}$	RAW 264.7 cells	0.73 nM (LoD)	129
FMH NPs-HE	$O_2^{\bullet-}$	HeLa cells	80 nM (LoD)	136
SOD@ATP/Tb-CPBA	$O_2^{\bullet-}$	Serum	25 nM (LoD)	138

Abbreviations: AuNPs, gold nanoparticles; CPBA, carboxyphenylboronic acid; CONER, Coumarin-neutral red; DBZTC, dibenzothiazolinecyclohexene; FAM, carboxyfluorescein; LoD, limit of detection; LoQ, limit of quantitation; MSN, mesoporous silica nanocontainer; SOD, superoxide dismutase; ssDNA, single-stranded DNA.

of LoD/LoQ than that of other nanoprobes, which could be ascribed to their unique background-free UCL analysis approach. Applications of these nanoprobes for $O_2^{\bullet-}$ and $\bullet OH$ detection have also been well demonstrated in biological fluid (sera) and imaging in living cells and animals. Although significant progress has been made in recent years, there is yet some room for the future precise detection and analysis of the level and distribution of $O_2^{\bullet-}$ and $\bullet OH$ in living organisms.

Although biological roles of ODFRs in the development of some diseases remain unclear, oxidative stress derived from the elevated level of reactive $O_2^{\bullet-}$ and $\bullet OH$ is closely related to damage of biological components. Due to their extreme reactivity, ODRFs reacts with many biomolecules quickly after their generation, while these oxidations are hardly to be quantitatively tracked. This requires the development of reliable bioanalytical methods for quickly and quantitatively monitoring these radicals in-situ and in vivo. Although a number of responsive nanoprobes have been developed and their feasibility in biological applications, particularly in imaging analysis, has been validated in recent years, real-time monitoring of the $O_2^{\bullet-}$ and $\bullet OH$ level in diseased tissues and during their treatment has not been achieved. In general, both $O_2^{\bullet-}$ and $\bullet OH$ concentrations are increased in diseased cells and tissues, thus more attempts can be paid to develop nanoprobes for simultaneous detection of $O_2^{\bullet-}$ and $\bullet OH$ to identify the diseased sites. Investigations of the effects of nanomaterial-based probes on the $O_2^{\bullet-}$ and $\bullet OH$ production during cellular internalization are also absent. This makes it unclear whether the variation of the $O_2^{\bullet-}$ and $\bullet OH$ level is derived from metabolic processes or from the cell response to the nanoprobe internalization.

Preclinical validation and translation of these responsive nanoprobes to be the diagnostic tools are also demanded. Although many nanoprobes have been developed, none of these probes are currently available for clinical trials for $O_2^{\bullet-}$ and $\bullet OH$ detection. This would require the close collaboration of analytical chemist, biologist, and clinical doctors to translate the responsive nanoprobes for better understanding of the properties and roles of $O_2^{\bullet-}$ and $\bullet OH$ in disease development and treatment.

CONFLICT OF INTEREST

ORCID

Run Zhang https://orcid.org/0000-0002-0943-824X
Zhi Ping Xu https://orcid.org/0000-0001-6070-5035

REFERENCES

1. B. Commoner, J. Townsend, G. E. Pake, *Nature* **1954**, *174*, 689.
2. K. Brieger, S. Schiavone, F. Miller, K.-H. Krause, *Swiss Med. Wkly.* **2012**, *142*, w13659.
3. H.-U. Simon, A. Haj-Yehia, F. Levi-Schaffer, *Apoptosis* **2000**, *5*, 415.
4. B. D'Autréaux, M. B. Toledano, *Nat. Rev. Mol. Cell Biol.* **2007**, *8*, 813.
5. H. Kawagishi, T. Finkel, *Nat. Med.* **2014**, *20*, 711.
6. A. A. Alfadda, R. M. Sallam, *J. Biomed. Biotechnol.* **2012**, *2012*, 936486.
7. X. Chen, X. Tian, I. Shin, J. Yoon, *Chem. Soc. Rev.* **2011**, *40*, 4783.
8. D. Andina, J.-C. Leroux, P. Luciani, *Chem-Eur. J.* **2017**, *23*, 13549.
9. L. Wu, A. C. Sedgwick, X. Sun, S. D. Bull, X.-P. He, T. D. James, *Acc. Chem. Res.* **2019**, *52*, 2582.
10. D. Closa, E. Folch-Puy, *IUBMB Life* **2004**, *56*, 185.
11. M. Martínez-Cayuela, *Biochimie* **1995**, *77*, 147.
12. H. Ahsan, A. Ali, R. Ali, *Clin. Exp. Immunol.* **2003**, *131*, 398.
13. L. A. Pham-Huy, H. He, C. Pham-Huy, *Int. J. Biomed. Sci.* **2008**, *4*, 89.
14. N. Sharma, *Biol. Med.* **2014**, *6*, 1.
15. J. M. McCord, *Am. J. Med.* **2000**, *108*, 652.
16. B. Halliwell, M. V. Clement, L. H. Long, *FEBS Lett.* **2000**, *486*, 10.
17. M. Valko, M. Izakovic, M. Mazur, C. J. Rhodes, J. Telser, *Mol. Cell. Biochem.* **2004**, *266*, 37.
18. S. Bedwell, R. Dean, W. Jessup, *Biochem. J.* **1989**, *262*, 707.
19. W. Droge, *Physiol. Rev.* **2002**, *82*, 47.
20. M. Valko, D. Leibfritz, J. Moncol, M. T. Cronin, M. Mazur, J. Telser, *Int. J. Biochem. Cell Biol.* **2007**, *39*, 44.
21. W. Dröge, *Physiol. Rev.* **2002**, *82*, 47.
22. R. Zhang, J. Yong, J. Yuan, Z. Ping Xu, *Coord. Chem. Rev.* **2020**, *408*, 213182.
23. G. Novelli, P. Angiolini, P. Livi, E. Paternostro, *Resuscitation* **1989**, *18*, 195.
24. H. Sies, E. Cadenas, *Philos. Trans. R. Soc. B* **1985**, *311*, 617.
25. B. Halliwell, J. M. Gutteridge, *Free Radicals in Biology and Medicine*. Oxford University Press, Oxford **2015**.
26. A. Valavanidis, T. Vlachogianni, C. Fiotakis, *J. Environ. Sci. Health, Part C: Toxicol. Carcinog.* **2009**, *27*, 120.
27. L. J. Kroese, P. G. Scheffer, *Curr. Atheroscler. Rep.* **2014**, *16*, 452.
28. T. Hofer, C. Badouard, E. Bajak, J.-L. Ravanat, Å. Mattsson, I. A. Cotgreave, *Biol. Chem.* **2005**, *386*, 333.
29. Y. Nakabeppu, D. Tsuchimoto, H. Yamaguchi, K. Sakumi, *J. Neurosci. Res.* **2007**, *85*, 919.
30. A. Sliwinska, D. Kwiatkowski, P. Czarny, M. Toma, P. Wigner, J. Drzewoski, K. Fabianowska-Majewska, J. Szemraj, M. Maes, P. Galecki, *J. Neurol. Sci.* **2016**, *368*, 155.
31. W. Martinet, G. De Meyer, A. Herman, M. Kockx, *Eur. J. Clin. Invest.* **2004**, *34*, 323.
32. C. Liu, X. Gao, J. Yuan, R. Zhang, *TrAC, Trends Anal. Chem.* **2020**, *133*, 116092.
33. S. Gaweł, M. Wardas, E. Niedworok, P. Wardas, *Wiadomosci Lekarskie* **2004**, *57*, 453.
34. L. J. Marnett, *Mutat. Res., Fundam. Mol. Mech. Mutagen.* **1999**, *424*, 83.
35. H. Esterbauer, K. H. Cheeseman, *Methods Enzymol.* **1990**, *186*, 407.
36. H. Bartsch, J. Nair, *Cancer Detect. Prev.* **2004**, *28*, 385.
37. B. S. Berlett, E. R. Stadtman, *J. Biol. Chem.* **1997**, *272*, 20313.
38. D. A. Butterfield, T. Koppal, B. Howard, R. Subramaniam, N. Hall, K. Hensley, S. Yatin, K. Allen, M. Aksenov, M. Aksenova, *Ann. NY Acad. Sci.* **1998**, *854*, 448.
39. E. Floor, M. G. Wetzel, *J. Neurochem.* **1998**, *70*, 268.
40. C. Smith, J. M. Carney, P. Starke-Reed, C. Oliver, E. Stadtman, R. Floyd, W. Markesbery, *Proc. Natl. Acad. Sci. U. S. A.* **1991**, *88*, 10540.
41. M. Chapman, B. Rubin, R. Gracy, *J. Rheumatol.* **1989**, *16*, 15.
42. A. Garcia-Garcia, H. Rodriguez-Rocha, N. Madayiputhiya, A. Pappa, M. I Panayiotidis, R. Franco, *Curr. Mol. Med.* **2012**, *12*, 681.
43. J. Lunec, *Ann. Clin. Biochem.* **1990**, *27*, 173.
44. R. A. Greenwald, W. W. Moy, *Arthritis Rheum.* **1980**, *23*, 455.
45. F. Collin, *Int. J. Mol. Sci.* **2019**, *20*, 2407.
46. A. Dąbrowsi, A. Gabryelewicz, U. Wereszczyńska-Siemeątkowska, L. Chyczewski, *Scand. J. Gastroenterol.* **1988**, *23*, 1245.
47. H. Sanfey, G. B. Bulkley, J. L. Cameron, *Ann. Surg.* **1984**, *200*, 405.
48. J. M. McCord, *New Engl. J. Med.* **1985**, *312*, 159.
49. M. J. P. Arthur, I. S. Bentley, A. R. Tanner, P. K. Saunders, G. H. Millward-Sadler, R. Wright, *Gastroenterology* **1985**, *89*, 1114.
50. B. Hammond, M. L. Hess, *J. Am. Coll. Cardiol.* **1985**, *6*, 215.
51. J. L. Zweier, M. A. H. Talukder, *Cardiovasc. Res.* **2006**, *70*, 181.
52. F. Bray, J. Ferlay, I. Soerjomataram, R. L. Siegel, L. A. Torre, A. Jemal, *Ca-Cancer J. Clin.* **2018**, *68*, 394.
53. R. Cairns, I. Harris, S. McCracken, T. Mak, *Cold Spring Harbor Symp. Quant. Biol.*, Cold Spring Harbor Laboratory, Cold Spring Harbor, NY **2011**, 299.
54. S. S. Brar, Z. Corbin, T. P. Kennedy, R. Hemendinger, L. Thornton, B. Bommarius, R. S. Arnold, A. R. Whorton, A. B. Sturrock, T. P. Huecksteadt, M. T. Quinn, K. Krenitsky, K. G. Ardie, J. D. Lambeth, J. R. Hoidal, *Am. J. Physiol. Cell Physiol.* **2003**, *285*, C353.
55. T. G. C. Murrell, *Med. Hypotheses* **1991**, *36*, 389.
56. H. Esme, M. Cemek, M. Sezer, H. Saglam, A. Demir, H. Melek, M. Unlu, *Respirology* **2008**, *13*, 112.
57. J. Opanuraks, C. Boonla, C. Saelim, W. Kittikowit, P. Sumpatanukul, C. Honglertsakul, P. Tosukhowong, *Asian Biomed.* **2010**, *4*, 703.
58. W. K. Subczynski, J. S. Hyde, *Biophys. J.* **1983**, *41*, 283.
59. E. Mariani, M. C. Polidori, A. Cherubini, P. Mecocci, *J. Chromatogr. B* **2005**, *827*, 65.
60. M. Pollack, C. Leeuwenburgh, *Handbook of Oxidants and Antioxidants in Exercise*, Vol. *30*, Elsevier Science B.V., Amsterdam **1999**, p. 881.
61. A. A. Farooqui, L. A. Horrocks, *Cell. Mol. Neurobiol.* **1998**, *18*, 599.
62. W. J. Huang, X. Zhang, W. W. Chen, *Biomed. Rep.* **2016**, *4*, 519.

63. J. Blesa, I. Trigo-Damas, A. Quiroga-Varela, V. R. Jackson-Lewis, *Front. Neuroanat.* **2015**, *9*, 91.

64. S. E. Browne, M. F. Beal, *Antioxid. Redox Signaling* **2006**, *8*, 2061.

65. Y. Gilgun-Sherki, E. Melamed, D. Offen, *J. Neurol.* **2004**, *251*, 261.

66. H.-C. Huang, Z.-F. Jiang, *J. Alzheimer's Dis.* **2009**, *16*, 15.

67. B. Uttara, A. V. Singh, P. Zamboni, R. Mahajan, *Curr. Neuropharmacol.* **2009**, *7*, 65.

68. W. R. Markesbery, M. A. Lovell, *Neurobiol. Aging* **1998**, *19*, 33.

69. M. Neely, K. Sidell, D. Graham, T. Montine, *J. Neurochem.* **1999**, *72*, 2323.

70. D. A. Bosco, D. M. Fowler, Q. Zhang, J. Nieva, E. T. Powers, P. Wentworth, R. A. Lerner, J. W. Kelly, *Nat. Chem. Biol.* **2006**, *2*, 249.

71. Z. I. Alam, S. E. Daniel, A. J. Lees, D. C. Marsden, P. Jenner, B. Halliwell, *J. Neurochem.* **1997**, *69*, 1326.

72. C. Olanow, *Neurology* **1990**, *40*, 32.

73. A. Kikuchi, A. Takeda, H. Onodera, T. Kimpara, K. Hisanaga, N. Sato, A. Nunomura, R. J. Castellani, G. Perry, M. A. Smith, *Neurobiol. Dis.* **2002**, *9*, 244.

74. M. L. Selley, *Free Radicals Biol. Med.* **1998**, *25*, 169.

75. T. Bahorun, M. Soobrattee, V. Luximon-Ramma, O. Aruoma, *Int. J. Med. Update* **2006**, *1*, 25.

76. G. Csányi, F. J. Miller Jr., *Int. J. Mol. Sci.* **2014**, *15*, 6002.

77. K. Prasad, J. Kalra, *Angiology* **1989**, *40*, 835.

78. R. J. Korthuis, D. N. Granger, M. I. Townsley, A. E. Taylor, *Circ. Res.* **1985**, *57*, 599.

79. H. S. Smith, A. R. Smith, P. Seidner, *Pain Physician* **2011**, *14*, E427.

80. M. Veselinovic, N. Barudzic, M. Vuletic, V. Zivkovic, A. Tomic-Lucic, D. Djuric, V. Jakovljevic, *Mol. Cell. Biochem.* **2014**, *391*, 225.

81. P. Vasanthi, G. Nalini, G. Rajasekhar, *Int. J. Rheum. Dis.* **2009**, *12*, 29.

82. S. Mateen, S. Moin, A. Q. Khan, A. Zafar, N. Fatima, *PLoS One* **2016**, *11*, e0152925.

83. B. Tang, N. Zhang, Z. Chen, K. Xu, L. Zhuo, L. An, G. Yang, *Chem. Eur. J.* **2008**, *14*, 522.

84. B. Ma, M. Lu, B.-Y. Yu, J. Tian, *RSC Adv.* **2018**, *8*, 22062.

85. Y. Zhou, S. Yang, Y. Xiao, Z. Zou, Z. Qing, J. Liu, R. Yang, *Anal. Chem.* **2019**, *91*, 15179.

86. T. Chen, Y. Hu, Y. Cen, X. Chu, Y. Lu, *J. Am. Chem. Soc.* **2013**, *135*, 11595.

87. L. Zhang, R.-P. Liang, S.-J. Xiao, J.-M. Bai, L.-L. Zheng, L. Zhan, X.-J. Zhao, J.-D. Qiu, C.-Z. Huang, *Talanta* **2014**, *118*, 339.

88. C. M. Gonzalez, M. Iqbal, M. Dasog, D. G. Piercey, R. Lockwood, T. M. Klapötke, J. G. C. Veinot, *Nanoscale* **2014**, *6*, 2608.

89. Q. Zhao, R. Zhang, D. Ye, S. Zhang, H. Chen, J. Kong, *ACS Appl. Mater. Interfaces* **2017**, *9*, 2052.

90. S. Liu, J. Zhao, K. Zhang, L. Yang, M. Sun, H. Yu, Y. Yan, Y. Zhang, L. Wu, S. Wang, *Analyst* **2016**, *141*, 2296.

91. M. King, R. Kopelman, *Sens. Actuators. B* **2003**, *90*, 76.

92. G. M. Ganea, P. E. Kolic, B. El-Zahab, I. M. Warner, *Anal. Chem.* **2011**, *83*, 2576.

93. D. Zhou, H. Huang, Y. Wang, Y. Wang, Z. Hu, X. Li, *J. Mater. Chem. B* **2019**, *7*, 3737.

94. B. Tang, L. Zhang, Y. Geng, *Talanta* **2005**, *65*, 769.

95. X. Hai, Z. Guo, X. Lin, X. Chen, J. Wang, *ACS Appl. Mater. Interfaces* **2018**, *10*, 5853.

96. R. Liu, L. Zhang, Y. Chen, Z. Huang, Y. Huang, S. Zhao, *Anal. Chem.* **2018**, *90*, 4452.

97. R. Zhang, B. Song, J. Yuan, *TrAC, Trends Anal. Chem.* **2018**, *99*, 1.

98. W. Zhang, Y. Liu, Q. Gao, C. Liu, B. Song, R. Zhang, J. Yuan, *Chem. Commun.* **2018**, *54*, 13698.

99. X. Jia, Q. Chen, Y. Yang, Y. Tang, R. Wang, Y. Xu, W. Zhu, X. Qian, *J. Am. Chem. Soc.* **2016**, *138*, 10778.

100. D. Wu, L. Chen, Q. Xu, X. Chen, J. Yoon, *Acc. Chem. Res.* **2019**, *52*, 2158.

101. M. Cong, N. Siraj, N. Bhattarai, P. E. Kolic, K. S. McCarter, P. K. Chhotaray, I. M. Warner, *Sens. Actuators. B* **2018**, *257*, 993.

102. Q. Su, W. Feng, D. Yang, F. Li, *Acc. Chem. Res.* **2017**, *50*, 32.

103. C. Duan, L. Liang, L. Li, R. Zhang, Z. P. Xu, *J. Mater. Chem. B* **2018**, *6*, 192.

104. Z. Li, H. Yuan, W. Yuan, Q. Su, F. Li, *Coord. Chem. Rev.* **2018**, *354*, 155.

105. Q. Guo, Y. Liu, Q. Jia, G. Zhang, H. Fan, L. Liu, J. Zhou, *Anal. Chem.* **2017**, *89*, 4986.

106. M. Zhao, F. Xu, L. Wang, H. Chen, *Analyst* **2020**, *145*, 530.

107. Z. Li, T. Liang, S. Lv, Q. Zhuang, Z. Liu, *J. Am. Chem. Soc.* **2015**, *137*, 11179.

108. X. Song, J. Zhang, Z. Yue, Z. Wang, Z. Liu, S. Zhang, *Anal. Chem.* **2017**, *89*, 11021.

109. S. Mondal, M. E. De Anda Reyes, U. Pal, *RSC Adv.* **2017**, *7*, 8633.

110. G. Yu, N. Feng, D. Zhao, H. Wang, Y. Jin, D. Liu, Z. Li, X. Yang, K. Ge, J. Zhang, *Sci. China: Life Sci.* **2021**, *64*, 434.

111. Q. Mei, Y. Li, B. N. Li, Y. Zhang, *Biosens. Bioelectron.* **2015**, *64*, 88.

112. B. Li, Z. He, H. Zhou, H. Zhang, T. Cheng, *Chin. Chem. Lett.* **2017**, *28*, 1929.

113. Y. Liu, Q. Jia, Q. Guo, A. Jiang, J. Zhou, *Anal. Chem.* **2017**, *89*, 12299.

114. K. Setsukinai, Y. Urano, K. Kakinuma, H. J. Majima, T. Nagano, *J. Biol. Chem.* **2003**, *278*, 3170.

115. Y. Xiao, Z. Ye, G. Wang, J. Yuan, *Inorg. Chem.* **2012**, *51*, 2940.

116. Y. Tong, X. Huang, M. Lu, B.-Y. Yu, J. Tian, *Anal. Chem.* **2018**, *90*, 3556.

117. M. Zhuang, C. Ding, A. Zhu, Y. Tian, *Anal. Chem.* **2014**, *86*, 1829.

118. Z. Li, L. Xiao, *Anal. Methods-UK* **2017**, *9*, 1920.

119. X. Liu, M. Ran, G. Liu, X. Liu, Z. Xue, X. Lu, *Talanta* **2018**, *186*, 248.

120. H. Yang, J. Hou, Z. Wang, T. Zhang, C. Xu, *Biosens. Bioelectron.* **2018**, *117*, 429.

121. H. Liang, H. Liu, B. Tian, R. Ma, Y. Wang, *Microchim. Acta* **2020**, *187*, 484.

122. O. Adegoke, E. Antunes, T. Nyokong, *J. Photochem. Photobiol., A* **2013**, *257*, 11.

123. J. Han, Z. Liu, Y. Guo, G.-C. Han, W. Li, S. Chen, S. Zhang, *J. Photochem. Photobiol., A* **2017**, *349*, 1.

124. R. Zhang, J. Yuan, *Acc. Chem. Res.* **2020**, *53*, 1316.

125. Y. Song, J. Hao, D. Hu, M. Zeng, P. Li, H. Li, L. Chen, H. Tan, L. Wang, *Sens. Actuators. B* **2017**, *238*, 938.

126. L. Yang, Y. Song, M. Zeng, Y. Du, B. Peng, Z. Huang, L. Wang, *Talanta* **2019**, *191*, 74.

127. N. Liu, J. Hao, K. Cai, M. Zeng, Z. Huang, L. Chen, B. Peng, P. Li, L. Wang, Y. Song, *Luminescence* **2018**, *33*, 119.

128. J. J. Gao, K. H. Xu, B. Tang, L. L. Yin, G. W. Yang, L. G. An, *FEBS J.* **2007**, *274*, 1725.

129. N. Li, H. Wang, M. Xue, C. Chang, Z. Chen, L. Zhuo, B. Tang, *Chem. Commun.* **2012**, *48*, 2507.

130. L. Yang, Y. Chen, Z. Yu, W. Pan, H. Wang, N. Li, B. Tang, *ACS Appl. Mater. Interfaces* **2017**, *9*, 27512.

131. X. Gao, C. Ding, A. Zhu, Y. Tian, *Anal. Chem.* **2014**, *86*, 7071.

132. H. Huang, F. Dong, Y. Tian, *Anal. Chem.* **2016**, *88*, 12294.

133. W. Pan, H. Wang, L. Yang, Z. Yu, N. Li, B. Tang, *Anal. Chem.* **2016**, *88*, 6743.

134. Q. Lu, D. Ericson, Y. Song, C. Zhu, R. Ye, S. Liu, J. A. Spernyak, D. Du, H. Li, Y. Wu, Y. Lin, *ACS Appl. Mater. Interfaces* **2017**, *9*, 23325.

135. R. Cheng, F. Kong, L. Tong, X. Liu, K. Xu, B. Tang, *Anal. Chem.* **2018**, *90*, 8116.

136. Y. Zhou, J. Ding, T. Liang, E. S. Abdel-Halim, L. Jiang, J.-J. Zhu, *ACS Appl. Mater. Interfaces* **2016**, *8*, 6423.

137. Y. Du, Y. Song, J. Hao, K. Cai, N. Liu, L. Yang, L. Wang, *Talanta* **2019**, *198*, 316.

138. Y. Weng, Q. Zhu, Z.-Z. Huang, H. Tan, *ACS Appl. Mater. Interfaces* **2020**, *12*, 30882.

AUTHOR BIOGRAPHIES

Jianping Liu started her PhD in Australian Institute for Bioengineering and Nanotechnology, The University of Queensland (AIBN, UQ) in July 2017, after successfully completing a master's degree in School of Chemical Engineering and Technology, Tianjin University. Under the supervision of Prof. Zhi Ping (Gordon) Xu and Dr. Run Zhang, her PhD project aims to develop a novel organic–inorganic hybrid nanocomposite system as co-delivery platform to enhance cancer treatment efficiency and prevent tumor metastasis via the combinational pathway.

Miaomiao Wu completed her master's degree in the Frontier Institute of Science and Technology jointly with the College of Science, Xi'an Jiaotong University in 2019. She has been a PhD student in Australian Institute for Bioengineering and Nanotechnology, The University of Queensland (AIBN, UQ) since 2021 under the supervision of Dr. Run Zhang and Prof Zhi Ping (Gordon) Xu. She is interested in developing novel nanoplatforms for biological applications, including bioimaging and cancer therapy.
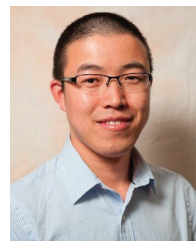
Run Zhang received his PhD from the Dalian University of Technology in 2012. He was a postdoctoral fellow and then a three years Macquarie University Research Fellow (MQRF) at MQ in 2012–2015. He joined the Australian Institute for Bioengineering and Nanotechnology, The University of Queensland (AIBN, UQ) in 2016. Here, he was awarded an ARC DECRA Fellow in 2017–2019 and now a NHMRC Emerging Leadership Fellow. His research interest focuses on the development of responsive molecules/nanomaterials for biosensing and imaging, early disease detection and treatment.

Prof Zhi Ping (Gordon) Xu is a senior group leader at the Australian Institute for Bioengineering and Nanotechnology, The University of Queensland. He obtained his BSc in the University of Science and Technology of China in 1988, and his PhD in the National University of Singapore in 2001. He is an expert in synthesis, characterization and applications of anionic clays, that is, layered double hydroxides and related nanomaterials (such as CaP and silica nanoparticles). His current research focuses on developing clay nanoparticles and related hybrids for drug/gene/vaccine delivery to treat tumor and infectious diseases, plant protection, and bioimaging and diagnosis.